ACS Sustainable Chemistry & Engineering

Research Article

pubs.acs.org/journal/ascecg

Homocomposites of Polylactide (PLA) with Induced Interfacial Stereocomplex Crystallites

Veluska Arias, Karin Odelius, Anders Höglund, and Ann-Christine Albertsson*

Department of Fibre and Polymer Technology, KTH Royal Institute of Technology, SE-100 44 Stockholm, Sweden

Supporting Information

ABSTRACT: The demand for "green" degradable composite materials increases with growing environmental awareness. The key challenge is achieving the preferred physical properties and maintaining their eco-attributes in terms of the degradability of the matrix and the filler. Herein, we have designed a series of "green" homocomposites materials based purely on polylactide (PLA) polymers with different structures. Film-extruded homocomposites were prepared by melt-blending PLA matrixes (which had different degrees of crystallinity) with PLLA and PLA stereocomplex (SC) particles. The PLLA and SC particles were spherical and with 300−500 nm size. Interfacial crystalline structures in the form of stereocomplexes were obtained for certain particulate-homocomposite formulations. These SC crystallites were found at the particle/matrix interface when adding PLLA particles to a PLA matrix with D-lactide units, as confirmed by XRD and DSC data analyses. For all homocomposites, the PLLA and SC particles acted as nucleating agents and enhanced the crystallization of the PLA matrixes. The SC particles were more rigid and had a higher Young's modulus compared with the PLLA particles. The mechanical properties of the homocomposites varied with particle size, rigidity, and the interfacial adhesion between the particles and the matrix. An improved tensile strength in the homocomposites was achieved from the interfacial stereocomplex formation. Hereafter, homocomposites with tunable crystalline arrangements and subsequently physical properties, are promising alternatives in strive for eco-composites and by this, creating materials that are completely degradable and sustainable.

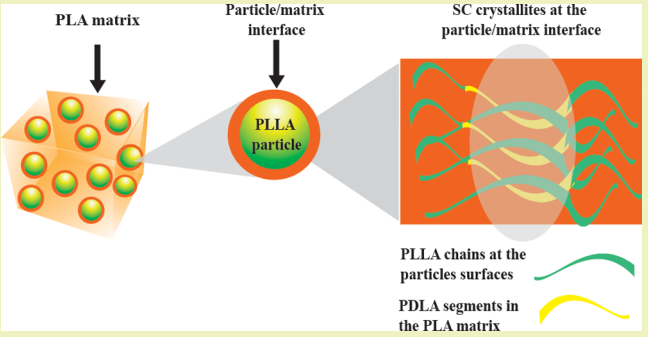

KEYWORDS: *Composites, Biodegradable, Morphology, Particles, Stereocomplexation, Interface*

INTRODUCTION

Ecological trends work toward the use of "green" composites as substitutes for traditional plastics. These materials are environmentally compatible without sacrificing performance. Composites currently available on the market aim for long-term durability as prime requirement. Therefore, they often contain nondegradable polymers such as epoxies and polyurethane reinforced with fibers (graphite, aramid, and glass), and due to their inherent heterogeneous nature the recycling processes for these materials are limited. In light of this, biobased and degradable polylactide (PLA) polymers are an attractive "green" alternative for composite materials. PLA has proven to degrade in different profiles and rates depending on the applied bulk modification.[1,2] The versatility of the lactide monomer has allowed the creation of new materials with unique architectures, mechanical and thermal properties.[3−6] Furthermore, by taking advantage of the hydrolysis process suffered by PLA at elevated temperatures, chemical recycling has resulted in high yield of monomer recovery.[7]

Composites are materials that consist of two or more chemically and/or physically different phases separated by a distinct interface. The phases are combined to achieve properties that cannot be attained by the individual constituents. The constituents retain their separate identities in the composite materials and work together to result in the necessary mechanical strength.[8] On this basis, we define a homocomposite as the combination of two physically distinct phases of the identical material separated by a particular interphase. The interfacial microstructure of a polymer composite (formed at the interface between solid-melt and solid−solid by thermomechanical mechanisms) is a research topic of great importance. For semicrystalline polymer matrixes, the crystalline structure near the interface needs to be considered as it affects the final properties of the composite.

Previous research has examined the crystalline structures near the interface between matrix and filler and their effect on interfacial adhesion and bond properties. Additionally, polymer processing methods such as extrusion and injection molding have been shown to influence the formation of interfacial crystalline arrangements.[9,10] Interfacial crystalline structures were found in injection molded polypropylene (PP), originating combined effects of the thermomechanical properties.[11] Leong et al. reported an increased interfacial adhesion between PP film and PP matrix when tuning the processing

Received: June 8, 2015
Revised: July 28, 2015
Published: July 29, 2015

DOI: 10.1021/acssuschemeng.5b00498
ACS Sustainable Chem. Eng. 2015, 3, 2220−2231

conditions and the interfacial crystalline structure was the decisive factor for controlling the mechanical properties.[12,13] Zhong et al. investigated the nucleation rate changes induced under different shear−stress conditions for PLA materials. The crystallization process under shear was enhanced, and the crystallization kinetics were accelerated with increasing shear rate and time.[14]

PLA-based composites have been reported with different fillers, including lignocellulosic materials,[15−17] natural fibers,[18−20] nanoclays,[21−23] nanotubes,[24,25] layered silicates[26,27] and nanoparticles of metals.[16,28] The successful preparation of multicomponent polymer-based materials relies on the strong interfacial adhesion from interactions between the phases.[1,29] Composites materials having different phases, such as polar fibers and a nonpolar or hydrophobic polymer matrix, require a defined strategy to improve compatibility and interfacial adhesion. Furthermore, the properties of PLA-based nanocomposites, such as PLA/nanoclay composites, strongly depend on the state of the filler in the composite where the dispersion in the matrix is one of the main problems. In this sense, PLA as filler could be a good candidate to be compatible within the PLA matrix. Single-polymer composites made from PLA materials have been previously reported with main focus on fiber type reinforcement, where the manufacturing process can significantly affect the fibers and by inference the properties of the composite.[30−32] In addition, small sized fillers, in the nanorange, increase the interfacial area and create a significant volume fraction of the interfacial layer. This layer exhibits properties different from the bulk polymer, even at low loadings. Filler loading below 5% (w/w) results in an effective enhancement of the nanocomposite properties.[33]

Oriented toward "green" composite materials, we have previously created PLA-based particles with tunable crystalline structures by spray droplet atomization. These particles could function as reinforcement materials in "green" composites.[3] Spherical PLA particles with a size of ∼400 nm and tunable crystalline arrangements were fabricated. By taking this to the next level, our aim is to use the well-defined PLA-based particles into PLA matrixes to create "green" homocomposite materials based solely on PLA. We hypothesize that combined thermomechanical effects could be achieved by the development of interfacial crystalline structures between PLA particles and PLA matrixes with different crystallinity. The relationship between the crystalline structures formed at the particle/matrix interface and the interfacial strength will enable greater control over the final properties of the material. Homocomposites with tunable physical properties are promising alternatives in strive for eco-composites to create materials that can be easily chemical recycled or fully degradable.

EXPERIMENTAL SECTION

Materials. The monomers L- and D-lactide (Boehringer Ingelheim, France) were purified by recrystallization three times in dry toluene. Ethylene glycol (EG; Sigma-Aldrich, Sweden) was used as the initiator. Stannous 2-ethylhexanoate ($Sn(Oct)_2$; 95%, Sigma-Aldrich, Sweden) was used as the catalyst. The solvents heptane (Fisher Scientific, Sweden), toluene (Fisher Scientific, Sweden) and chloroform (Fisher Scientific, Sweden) were used as received.

Polymer Synthesis. Poly(L-lactide) (PLLA) and poly(D-lactide) (PDLA) were synthesized using the ring-opening polymerization of L- and D-lactide. The catalyst was $Sn(Oct)_2$, and the initiator was EG. The reaction was performed in a thermostatically controlled oil bath at 110 °C for 72 h, as previously reported.[34] The content of D-lactide in the monomer feed ratio was set to 0, 5 and 7.5% (mol/mol) for the synthesis of PLA with varying isomeric compositions.

Particle Preparation Method. PLA particles were obtained as dry powders by spray drying polymers solutions using a laboratory-scale spray-dryer (Büchi Mini Spray Dryer B-290, Switzerland).[3] The feed rate was adjusted by setting the pump speed to 30%, the two-fluid nozzle had a diameter of 0.7 mm and the inlet temperature was maintained at 65 °C ± 3 °C for all samples. These settings resulted in an outlet temperature of 65 ± 3 °C. The air flow rate (700 Nl/h) and the aspirator at 100% (35 m^3/min) were constant. The spray-dried powders were collected and stored in a desiccator at room temperature. The polymer solutions were prepared in a concentration of 0.25 g material/100 mL chloroform. PLLA particles were prepared from the synthesized PLLA (M_n = 1.60 × 10^5 Da and $Đ$ = 1.2). SC particles were prepared from an equimolar mixture of the synthesized PLLA (M_n = 1.60 × 10^5 Da and $Đ$ = 1.2) and PDLA (M_n = 1.80 × 10^5 Da and $Đ$ = 1.1).

Homocomposite Preparation Method. The homocomposites were prepared by extrusion using a twin-screw mini extruder (DSM-Xplore 5 cm^3 Micro-Compounder, Model 2012). For the formulations that used matrixes with higher melting temperatures, the gradient temperatures from the feed throat to the die were 168, 170 and 170 °C. For the formulations that used matrixes with lower melting temperatures, the gradient temperatures were 158, 160 and 160 °C. The screw speed was 80 rpm during 3 min in counter-rotating mode. The homocomposites had a filler loading of 5% (w/w) for both PLLA and PLASC particles. The samples were dried overnight at 40 °C under vacuum before compounding. This drying minimized degradation during processing. The extruded materials were obtained as films by forcing the material through a film die with dimensions 35 mm width and 0.2 mm thickness.

Characterization Techniques. *Size Exclusion Chromatography (SEC).* The number-average molar mass (M_n) and the dispersity ($Đ$) of the PLA polymers were determined using a Verotech PL-GPC 50 Plus system with a PL-RI Detector and two Mixed-D (300 × 7.5 mm) columns from Varian. The samples were injected with a PL-AS RT Autosampler for PLGPC 50 Plus using chloroform as the mobile phase (1 mL/min, 30 °C). Polystyrene standards, with a narrow molar mass distribution in the range of 580−400 000 g/mol, were used for calibration. Corrections for flow rate fluctuations were performed using toluene as the internal standard.

Polarimetry. The D-isomer content in the synthesized PLA matrixes was measured by polarimetry using an AUTOPOL IV Automatic Polarimeter (Rudolph Research Analytical, New Jersey). The PLA materials were dissolved in chloroform at a concentration of 1 g/100 mL. Sample solutions were transferred to 100 mm cells and analyzed at a standard wavelength of λ = 589 nm. The D-isomer percentage was then calculated using the following equation:

$$\% = \frac{[\alpha]_{PLLA} - [\alpha]_{PDLLA}}{2[\alpha]_{PLLA}} \times 100 \quad (1)$$

where $[\alpha]_{PLLA}$ is the specific rotation for PLLA and $[\alpha]_{PDLLA}$ is the specific rotation for the unknown sample.[35]

Differential Scanning Calorimetry (DSC). The thermal properties of the particles were measured using DSC equipment (Mettler Toledo DSC 820 module). Approximately 5 mg of polymer was encapsulated in 40 μL aluminum crucibles without a pin. The temperature program was (I) heat from −20 to +270 °C, (II) cool to −20 °C and (III) heat for a second time to 270 °C. The heating and cooling rate was 10 °C/min under a nitrogen atmosphere (nitrogen flow rate 50 mL/min). The melting temperature (T_m) was noted as the maximum value of the melting peaks, and the glass transition temperature (T_g) was determined from the midpoint temperature of the glass transition. The approximate crystallinity of the materials was calculated according to eq 2.

$$w_c = \frac{\Delta H_f}{\Delta H_f^0} \times 100 \quad (2)$$

DOI: 10.1021/acssuschemeng.5b00498
ACS Sustainable Chem. Eng. 2015, 3, 2220−2231

Table 1. Matrixes, Molar Masses, Dispersity, Isomeric Content, Crystallinity before Extrusion and Physical Properties of the Particles (Size and Thermal Properties)

		M_n (Da, $\times 10^5$)[a]	$Đ$[a]	D-content[b] (mol %)	particle size (nm)[c]	particle size dispersity (nm)[c]	T_m (°C)[d]	w_c (%)[d]
matrix	PLA_{high}	0.85	1.2				171	57
	PLA_{med}	1.51	1.1	2.6 ± 0.4			150	27
	PLA_{low}	1.02	1.1	3.4 ± 0.1			143	5
filler	PLLA	1.60	1.2		443.4	0.2	176	57
	SC[e]				364.8	0.2	226	62

[a]Determined by SEC using $CHCl_3$ as the eluent and polystyrene standards. [b]Determined by polarimetry. [c]z-average value. [d]Determined by DSC. [e]PLLA with M_n = 1.60 × 10^5 Da and $Đ$ = 1.2 and PDLA with M_n = 1.80 × 10^5 Da and $Đ$ = 1.1.

where w_c is the degree of crystallinity and ΔH_f is the heat of fusion of the sample. The heat of fusion of a 100% crystalline PLA polymer (93 J/g)[2] and 100% PLA stereocomplex (102 J/g) is ΔH_f^0.[36]

Thermogravimetric Analysis (TGA). The thermal stability of the particles and homocomposite materials was evaluated using a TGA instrument (Mettler Toledo TGA/DSC 1 module). Approximately 5 mg of sample was loaded into a ceramic cup and heated from 25 to 600 °C at a rate of 10 °C/min under a nitrogen atmosphere (the nitrogen flow rate was 50 mL/min).

Scanning Electron Microscopy (SEM). The morphology of the surface area of the particles was evaluated using a Hitachi S-4800 SEM with an accelerating voltage of 1.5 kV. The samples were mounted on metal studs and were sputter-coated with gold−palladium using a Cressington 208HR sputter-coater unit.

Dynamic Light Scattering (DLS). The size of the particles was measured by dynamic light scattering (DLS) using a Zetasizer Nano ZS at 25 °C. Water solutions containing particles at a concentration of 1 mg/mL were ultrasonicated for 30 min and filtered using 1.2 μm nylon syringe filters.

Atomic Force Microscopy (AFM). The particles were topographically characterized using a Nanoscope IIIa multimode atomic force microscope (Digital Instruments, United States) with a 5346 EV scanner. A silicon-etched probe tip (TAP150, Bruker, United States) with a normal spring constant (k) of 5 N/m and a resonance frequency (f_0) of 150−200 kHz was used to scan the image in tapping mode. The surface of the materials was scanned from 1−2 Hz with a selected maximum sample size of 512 × 512 pixels. Mechanical measurements on the surface of the particles were performed using PeakForce Quantitive Nanomechanical Mapping mode (PeakForce QNM). The spring constant of the cantilever was calibrated three times using the thermal tune method and resulted in an average value of 4.6084 N/m. The cantilever was tested during the scanning of a PS/LDPE standard sample with known mechanical contact data to confirm the calibration. The obtained force profiles were analyzed using the Derjaguin−Muller−Toporov (DMT) model[37,38] with NanoScope Analysis software. The Young's modulus of the particles surface was obtained from the mechanical model.

X-ray Diffraction (XRD). The crystalline morphology of the homocomposite materials was analyzed by X-ray diffraction (XRD) using a PANalytical XPert Pro instrument with Cu Kα radiation (λ = 1.54 Å) generated at 45 kV and 45 mA. The spectra were recorded at 25 °C using a silicium monocrystal sample holder at a step size of 0.017°. The intensity in the spectra was measured as a function of 2θ in the angle range of 5−50°.

Tensile Testing. The mechanical properties of the homocomposites were evaluated by tensile testing. Tensile tests on the extruded films were performed using an INSTRON 5944 module according to the standard ASTM D638-10. Strips of 5 mm width and 50 mm length were cut from the films and five specimens were tested for each material. The measurement was performed with a 500 N load cell at a strain rate of 20 mm/min. The samples were preconditioned at 23 °C and 50% RH for 40 h according to the standard ASTM D618-08.

RESULTS AND DISCUSSION

Homocomposite Formation. Essential queries when designing "green" materials are to keep their eco-qualities while accomplishing the desired properties. Here, we designed a series of "green" homocomposites based solely on PLA materials. Particulate-homocomposites were prepared by combining PLA matrix that had different D-isomer contents and crystallinities with PLLA and PLA stereocomplex (SC) particles. The homocomposites had a filler loading of 5% (w/w) for both PLLA and PLASC particles. Interfacial stereocomplex crystalline arrangements between the particles and the matrix induced increased interfacial strength. The phenomenon resulted in unique mechanical and thermal properties for each system. The matrixes had high molar masses and low dispersity values before and after processing (Table 1). The matrixes were melt-blended with PLA-based particles prepared by spray-droplet atomization.[3] The spherical particles (PLLA and SC (Figure S1)) are distinguished by their crystalline arrangements, melting temperatures and degree of crystallinity. The highest values were observed for SC particles.[39] Six different systems of particulate-based homocomposite materials were prepared by a melt-blending process. The material's ID, e.g., PLA_{high}(SC), represents the polymer that was used as a matrix (PLA), the degree of crystallinity of the matrix (high) and the particulate filler used in the homocomposite preparation (SC). This notation is used throughout the Results and Discussion.

The M_n of the matrixes after processing (Table S1) demonstrated small alterations compared with the values obtained before processing (Table 1). This finding indicated that nondestructive melt-blending was achieved. The molar masses of the particulate-homocomposites were in the range of 0.8−1.5 × 10^5 Da with low dispersity values after extrusion. The extruded films exhibited different macrostructures depending on the PLA matrix used (Figure 1). In pure matrixes, a decrease in opacity was observed with decreased crystallinity: PLA_{high} > PLA_{med} > PLA_{low}. All three PLA(SC) homocomposites contained white dots dispersed in the matrix. PLA(PLLA) homocomposites appeared more similar to the pure PLA matrixes. This finding is likely because of an agglomeration of the SC particles during the melt-processing that induced some opacity in the PLA(SC) homocomposite. The smaller SC particle size, which increases the surface area to volume ratio, results in a tendency for agglomeration.[40]

Particulate-Homocomposites Crystallization Behavior. The incorporation of the particles into the matrixes, and the interfacial stereocomplex crystallites found at the particle/matrix interface of specific particulate-homocomposite materials, were confirmed by thermal analysis (Figure 2) and XRD diffraction patterns (Figure 3). PLA_{high}(SC) demonstrated two endothermic peaks at 174 and 223 °C. The latter peak corresponded to the SC particles with a T_m at 226 °C (Table 1 and Figure S2). No significant changes were observed when PLLA particles were added to the PLA_{high} matrix. A broadening in the endothermic melting peak was observed when PLA_{med}

DOI: 10.1021/acssuschemeng.5b00498
ACS Sustainable Chem. Eng. 2015, 3, 2220−2231

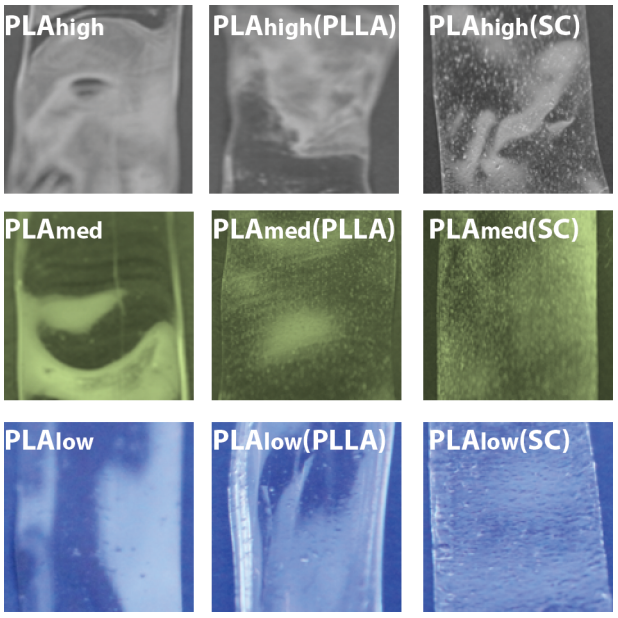

Figure 1. Images of the particulate-homocomposites and the pure matrixes after film extrusion.

was compared with PLA_{high}. This broadening most likely occurred because of the melting of different crystal conformations in the materials.[41] PLA_{med} and PLA_{low} are a combination of L-lactide and D-lactide isomers (Table 1) that disrupts crystal formation and results in a double endothermic peak in the thermogram. The addition of PLLA particles to PLA_{med} (PLA_{med}(PLLA)) induced the formation of a second endothermic melting peak at 220 °C. This indicates that SC crystallites were formed at the particle/matrix interface during the melt-processing of the homocomposites. For PLA_{med}(SC), two clear endothermic peaks were observed at 151 °C (matrix) and 217 °C (SC particles). PLA_{low} and PLA_{med} demonstrated a double melting peak that was more pronounced with the addition of particles. For PLA_{low}(PLLA), three endothermic peaks were observed at temperatures of 144 °C, 176 and 211 °C, corresponding to the PLA matrix, the PLLA particles and the SC crystallites, respectively. In the case of PLA_{low}(SC), two clear endothermic peaks appeared at 143 and 223 °C, corresponding to the matrix and the SC particles, respectively. Additionally, cold crystallization (CC) was observed in some of the formulations. Pure PLA_{med} exhibited CC, and a shift toward lower temperatures in the CC was observed after particle addition for PLA_{med}(PLLA) and PLA_{med}(SC). This finding is most likely because of a facilitated crystallization after particle addition. The identical phenomenon was observed for the PLA_{low} formulations. PLA_{low}(PLLA) and PLA_{low}(SC) demonstrated CC. The lowest temperature was exhibited by PLA_{low}(PLLA).

SC crystallites were formed in the PLA_{med}(PLLA) and PLA_{low}(PLLA) homocomposites, but not in the pure PLA_{med} and PLA_{low} matrixes, which are composed of nonequimolar L- and D-lactide units. This finding is explained by an oriented overgrowth of the SC crystalline phase on the surface of the particles. The particle surface acts as a substrate that is also crystalline.[42] Therefore, SC crystallites are formed at the interface between the PLLA particles and the PLA_{med} and PLA_{low} matrixes when the L-lactide units at the particles surface meet the D-lactide units in the matrix. This specific interfacial interaction between two distinct components is enhanced by an increase in chain mobility upon melting. The orientation of the particles as substrates may enhance the subsequent nucleation at the interface. These special crystallization conditions have been reported for homocrystallites of PLLA on the stereocomplex crystallites of PLLA and poly(L-lactide-*co*-D-lactide) (20/80) in a ratio of 80/20 that is crystallized from the melt.[43]

The particles enhanced the nucleation of a second crystalline phase, i.e., SC crystallites, by lowering the free energy of activation through the force field near the surface, which also depends on their spatial arrangements. The shear under extrusion facilitated the dispersion of the particles in the matrix and thus enhanced the interfacial complex formation. Simple physical blending of the components did not result in an interfacial complex upon melting during thermal analysis for PLA_{med}(PLLA). Furthermore, SC crystallites were not found in the pure matrixes, PLA_{med} and PLA_{low}, after melt-blending even when these matrixes are composed of L-lactide and D-lactide units. PLLA particles showed purely homocrystallites under thermal analysis. This confirms that the SC crystallites are only formed at the particle/matrix interphase. The SC crystallites could have also been formed during the DSC heating process. However, the thermograms represent the first heating scans that report the thermal history of the materials.

The interfacial complex formation is then explained by the increased crystallization of SC crystallites compared with homocrystallites because of the higher growth rate and density of the SC spherulites and the shorter induction period.[44] SC is preferred over homopolymer crystallization, even at the lower D-content in the PDLA phase in a PLLA-rich matrix.[45] The crystallization of the SC at the interface is most likely completed before the crystallization of the homopolymer begins. The excess of L-units in the interaction between the chains with identical configuration prevails, and they assemble separately to form homocrystallites in the matrix.

The thermal properties of the homocomposites were different depending on the composition (Table 2). For PLA_{high}, SC particles slightly increased the T_g, and no variation was observed for PLA_{high}(PLLA). The SC particles may reduce the chain mobility in the PLA_{high} matrix, thereby resulting in an increase in the T_g. The enthalpy of fusion (ΔH_f) increased for both PLA_{high}(PLLA) and PLA_{high}(SC) and resulted in increased crystallinity. The enhanced crystallization is because of the heterogeneous nucleation effect induced by the particles. This lowers the surface free energy barrier toward nucleation and allows crystallization to occur at higher temperatures upon cooling. Small content of high molar mass PDLA chains in a PLLA-rich matrix induces the formation of SC crystallites under nonisothermal crystallization. Racemic crystallites are formed over homocrystallites. These crystallites acted as nucleation sites and increased the number of PLLA spherulites and thus the overall crystallization rate.[46] In the case of PLA_{med}, the T_g did not vary with the addition of particles compared with the pure matrix. The ΔH_f and the w_c increased with the addition of both PLLA and SC particles. The highest values were observed for PLA_{med}(SC). The SC particles acted then as better nucleating agents than the PLLA particles. The smaller particle size demonstrates a higher nucleating effect (SC particles are smaller than the PLLA particles, Table 1). An identical trend was observed for PLA_{low}(PLLA) and PLA_{low}(SC). The T_m of PLA_{med}(PLLA) and PLA_{med}(SC), and PLA_{low}(PLLA) and PLA_{low}(SC) slightly decreased in comparison with their respective matrixes. The nucleating effect of the

DOI: 10.1021/acssuschemeng.5b00498
ACS Sustainable Chem. Eng. 2015, 3, 2220−2231

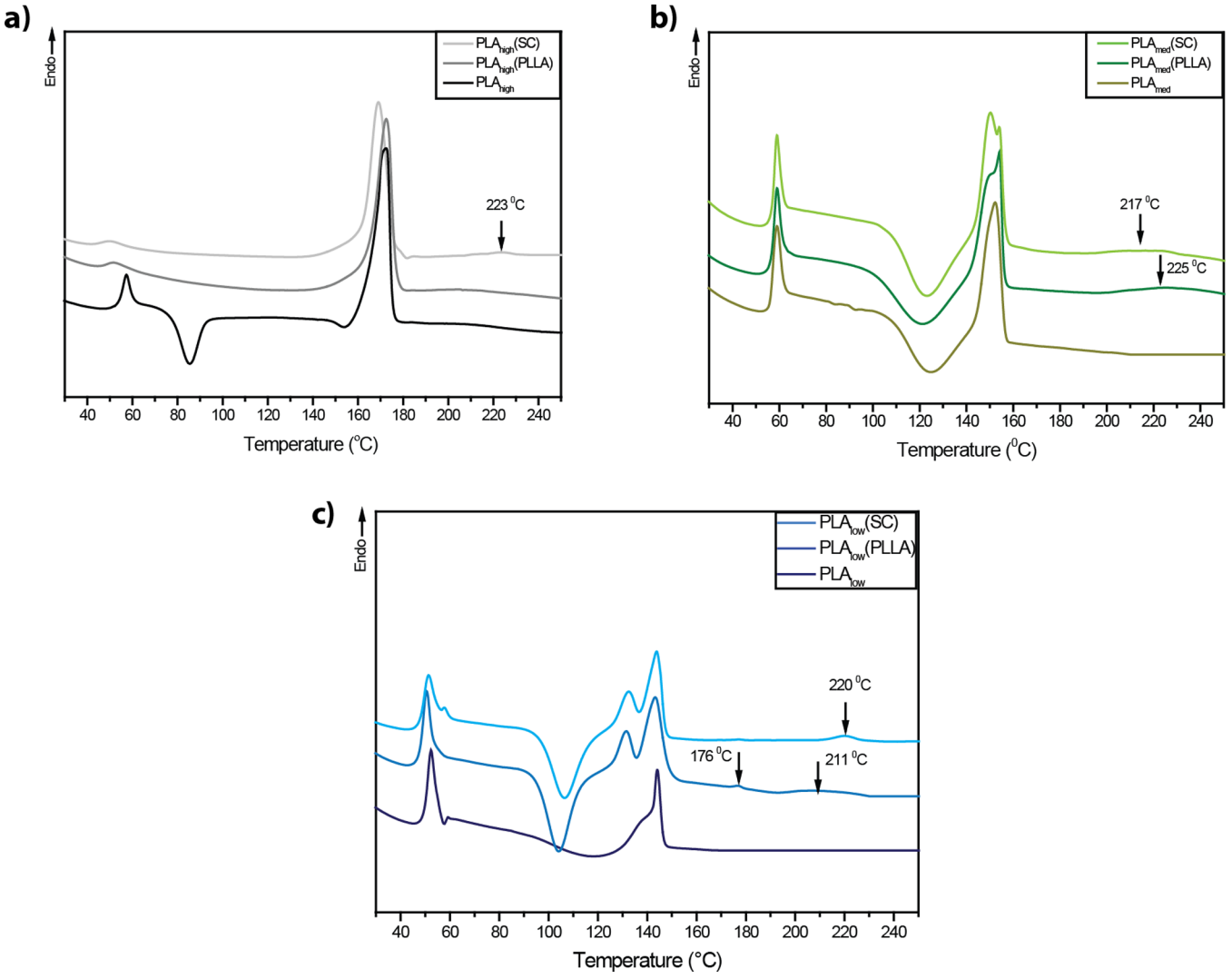

Figure 2. DSC thermograms of the first heating scan of (a) PLA_{high}, PLA_{high}(PLLA) and PLA_{high}(SC), (b) PLA_{med}, PLA_{med}(PLLA) and PLA_{med}(SC) and (c) PLA_{low}, PLA_{low}(PLLA) and PLA_{low}(SC).

particles enhances the crystallization process, lowers the crystallization temperature and results in lower T_m values.

Interfacial Crystalline Structure. The presence of SC crystallites in the homocomposites, formed at the interface between the PLLA particles and the PLA_{med} and PLA_{low} matrixes, was revealed by X-ray scattering profiles (Figure 3) confirming the results obtained from DSC data (Figure 2). The peaks in the X-ray patterns of the matrix materials, PLA_{high}, PLA_{med} and PLA_{low}, appeared at 2θ, with values of 17 and 19°. These peaks correspond to the α form of PLLA and PDLA crystallized in a pseudo-orthorhombic unit cell.[47] SC crystallites were observed at 2θ, with values of 12, 21 and 24°. These peaks correspond to PLA, crystallized in a triclinic unit cell, in which the L- and D-lactide segments are packed parallel in a helical conformation.[47] These results confirm the presence of SC particles in the homocomposites and the presence of SC crystallites formed at the interface. The crystallites are formed during the processing between pure PLLA particles mixed with a PLA matrix with D-lactide segments. Their presence is additionally confirmed by the thermograms of the homocomposites (Figure 2). This interfacial crystallite formation was induced during the film-making process. The films were obtained by hot-drawing directly after melt-blending. This process causes an increase in the surface area per unit molecule. This increase is achieved through the expansion of the chains, which in turn increases the probability of interaction between the PLLA chains at the particles surface and the PDLA segments in the matrix. The PLLA chains at the particle surface and the PDLA segments at the matrix arrange themselves side by side through strong hydrogen bonding interactions at the particle/matrix interface under the shear stress of processing (Scheme 1). This tight chain packing at the particle/matrix interface is referred to the SC structure. SC crystallites formed from the melt have been reported in hot-drawing PLA fibers.[48] SC or racemic crystallites can also be formed from the melt when PLLA and PDLA segments are in nonequimolar concentration. This formulation results in a mixture of racemic and homocrystallites because the racemic crystallites form more rapidly than do the homocrystallites.[49] Bai et al. reported SC crystallites at the interphase in blends of PLLA/elastomers containing PDLA units through melt-blending.[50]

Mechanical Properties. The formation of interfacial crystalline structures influences the mechanical properties (Figure 4). Incorporating a small weight percentage (5% (w/w)) of PLLA and SC particles into the different PLA matrixes resulted in significant variations in the mechanical properties

DOI: 10.1021/acssuschemeng.5b00498
ACS Sustainable Chem. Eng. 2015, 3, 2220−2231

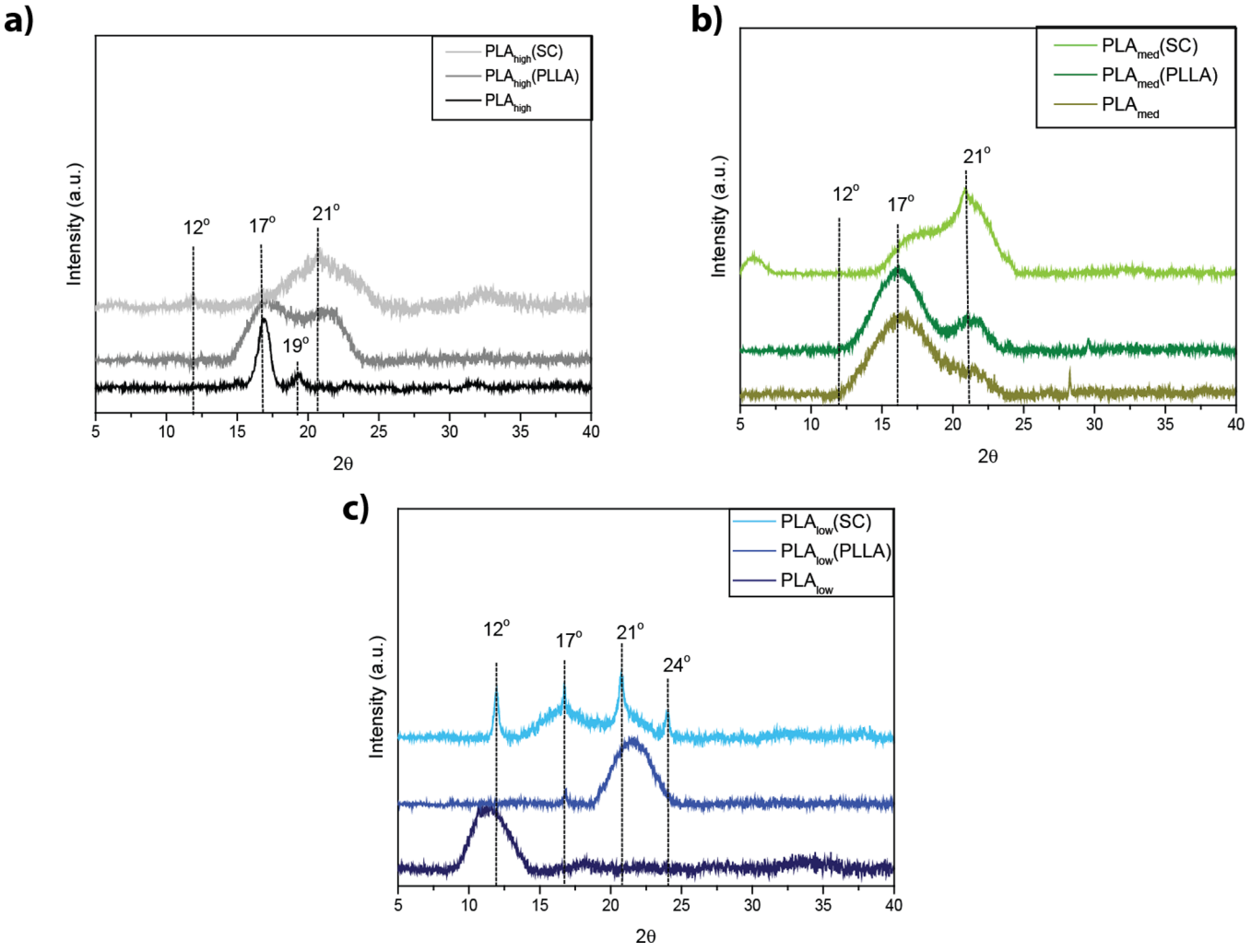

Figure 3. XRD patterns of the particulate-homocomposite materials: (a) PLA_{high}-based, (b) PLA_{med}-based and (c) PLA_{low}-based homocomposites.

Table 2. Thermal Properties of the Particulate-Homocomposite Materials after Extrusion[a]

	1st heating				
material	T_g (°C)	T_m (°C)	ΔH_f (J/g)	ΔH_{cc} (J/g)	w_c (%)
PLA_{high}	54.7 ± 0.3	169.7 ± 0.2	55.6 ± 0.9	23.1 ± 2	39.7 ± 1
PLA_{high}(PLLA)	54.7 ± 0.2	170.4 ± 0.5	54.9 ± 0.2		58.9 ± 0.2
PLA_{high}(SC)	56.6 ± 0.6	174.0 ± 0.3	56.9 ± 1.9		61.2 ± 1.0
PLA_{med}	53.6 ± 0.1	153.7 ± 0.3	26.7 ± 1.5	12.6 ± 1.2	15.7 ± 0.8
PLA_{med}(PLLA)	53.4 ± 0.3	150.5 ± 0.1	27.9 ± 0.5	9.6 ± 0.7	20.1 ± 1.0
PLA_{med}(SC)	53.3 ± 0.5	151.0 ± 0.4	31.4 ± 0.1	11.8 ± 0.8	23.7 ± 0.1
PLA_{low}	49.8 ± 0.2	144.3 ± 0.1	9.6 ± 0.3		10.3 ± 0.4
PLA_{low}(PLLA)	46.1 ± 0.3	143.9 ± 0.4	26.9 ± 1.5	15.2 ± 3	14.9 ± 1.6
PLA_{low}(SC)	46.6 ± 0.4	143.9 ± 0.4	35.1 ± 0.6	12.5 ± 3	20.7 ± 0.7

[a]Determined by DSC from the 1st heating scan.

between the homocomposites. The mechanical properties of the particulate-homocomposite materials demonstrated differences that depended on the particle size, particle nature (rigid or soft) and particle/matrix interfacial adhesion. These factors are discussed for each of the properties examined: Young's modulus, tensile strength and fracture toughness.

The E-modulus, after the addition of PLLA and SC particles, was improved for all homocomposites compared with the neat matrixes (Figure 4a). The E-modulus relates to the stiffness of the material in the elastic region during tensile testing. The stiffness is improved by the addition of particles that are more rigid than the matrix. PLA(SC) homocomposites demonstrated a higher E-modulus than did the PLA(PLLA) homocomposites. The E-modulus is less dependent on the particle size until a critical particle size is reached. Below this value, the effect of particle size on the E-modulus is more significant.[51] The differences in the E-modulus between PLA(SC) and PLA(PLLA) are attributed to the rigidity of the particles rather than the variation in size (~80 nm). Additionally, the particle/matrix interfacial adhesion has shown to have little effect in the E-

DOI: 10.1021/acssuschemeng.5b00498
ACS Sustainable Chem. Eng. 2015, 3, 2220−2231

Scheme 1. Schematic Representation of the Interfacial Complex Formation between the PLLA Chains at the Particle Surface and the PDLA Segments in the PLA Matrix

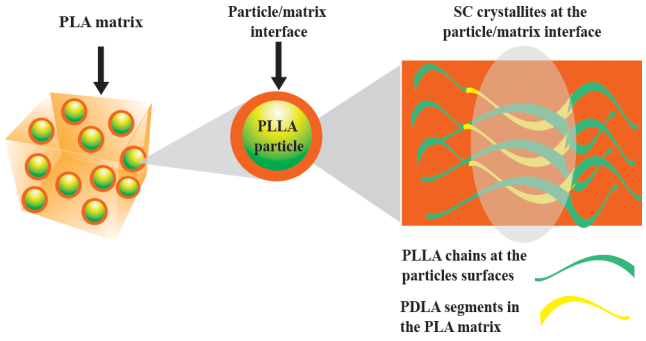

modulus.[52] Small differences in the E-modulus were observed for PLA_{med} and PLA_{low} after the addition of PLLA particles, although these materials demonstrated interfacial crystallite formation (Figures 2 and 3). The E-modulus is measured at relatively low deformation in which there is no sufficient dilation to cause interfacial separation between the matrix and the particle.

The rigidity of the particles resulted in clear differences in the E-modulus for the PLA(PLLA) and the PLA(SC) homocomposites. The SC particles demonstrated higher E-modulus (Figure 5) than did the PLLA particles most probably because of the high crystallinity values obtained during the stereocomplexation. During stereocomplexation, intermolecular crystallization dominates when blending PLLA and PDLA. This phenomenon results in increased tie chains between the crystallites.[53] Analysis of the pure PLLA and SC particles demonstrated average height values of 1.2 and 3.2 GPa (Figure 5), respectively.

Figure 5. Representative E-Modulus images of the PLLA particles (left) and the SC particles (right) used as fillers (AFM PeakForce QNM). All QNM images were scanned over an area of 1 × 1 μm.

Depending on the filler particles, the tensile strength of the homocomposites demonstrated a large variation within the matrixes (Figure 4b). The tensile strength is the maximum stress that the material can bear under uniaxial tensile loading.

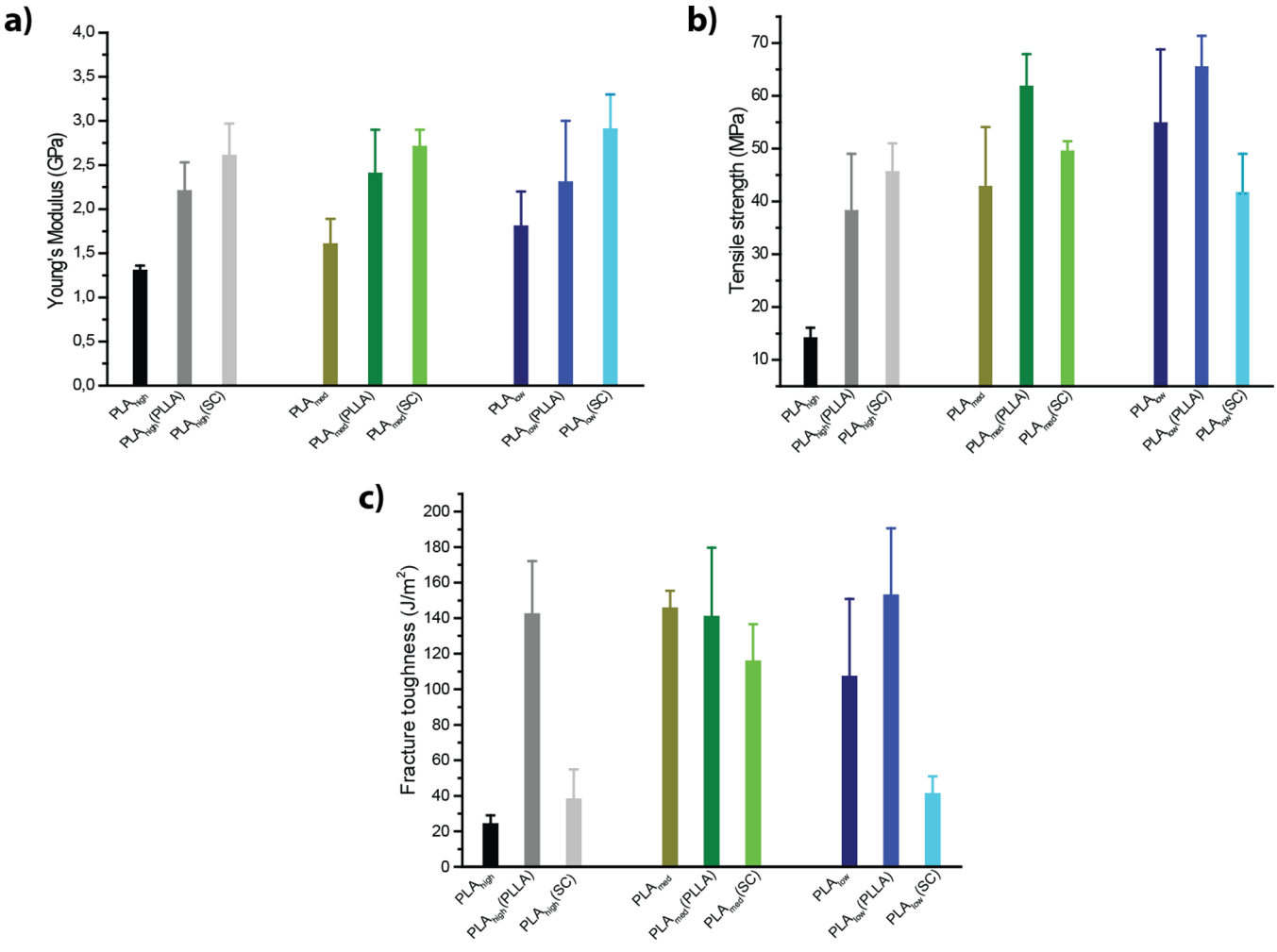

Figure 4. Homocomposite materials mechanical properties: (a) Young's modulus, (b) tensile strength and (c) toughness.

DOI: 10.1021/acssuschemeng.5b00498
ACS Sustainable Chem. Eng. 2015, 3, 2220−2231

For these homocomposites, the strength depends on the stress transfer between the matrix and the particle filler. Particle size and the particle/matrix interfacial adhesion affect the strength of the material. For PLA_{high}, the strength of the materials increased with decreasing the particle size: $PLA_{high} \ll PLA_{high}(PLLA) < PLA_{high}(SC)$. Smaller particles (such as SC particles) have a higher surface area, which results in a more efficient stress transfer. $PLA_{med}(PLLA)$ and $PLA_{low}(PLLA)$ had higher tensile strengths compared to $PLA_{med}(SC)$ and $PLA_{low}(SC)$. The interfacial adhesion had a larger effect than did the particle size. The adhesion strength at the particle/matrix interface defines the load transfer between the particle and the matrix. SC crystallites are formed at the interface between the PLLA particles and the PLA_{med} and PLA_{low} (Figures 2 and 3). The crystal formation at the interface contributed to the improved adhesion of the particles to the matrix. This adhesion increased the stress transfer between the components. Particle agglomeration may have affected the stress transfer between the particles and the matrix. The SC particles coalesced more readily than the PLLA particles in the homocomposites (Figure 1). This behavior resulted in the lower tensile strength values obtained for $PLA_{med}(SC)$ compared with $PLA_{med}(PLLA)$. The strong interfacial interaction between the PLLA particles in $PLA_{med}(PLLA)$ and the matrix may facilitate the dispersion of the filler in the matrix and obstructing possible agglomeration. This behavior was observed for the PLA_{low}-based materials. The tensile strengths of these homocomposites were $PLA_{low} < PLA_{low}(PLLA) > PLA_{low}(SC)$. The introduction of rigid SC particles into a polymer matrix results in a reduction in the strength of the material, but at the same time the crack propagation becomes more difficult. The particle loading also affects the strength of the material (Figure S3). Different amounts of SC particles, i.e., 5 and 10 wt %, were added to the PLA_{high} matrix. Increased brittleness was observed in the homocomposites that contained an increased particle amount. Mechanical testing was not possible for the film of $PLA_{high}(SC)$ with 10 wt % particles because of increased brittleness probably due to agglomeration of the particles. Smaller sized particles have a higher coalescent tendency that interrupts the stress transfer between the particle and the matrix and induce brittleness.[54]

The fracture toughness of the homocomposites differed for all of the particle−matrix combinations (Figure 4c). For PLA_{high}, the fracture toughness increased with the addition of PLLA particles. The addition of SC particles had no effect: $PLA_{high} \ll PLA_{high}(PLLA) \gg PLA_{high}(SC)$. For PLA_{med} and its homocomposites, the toughness slightly decreased with the addition of both particles in comparison with the matrix: $PLA_{med} \geq PLA_{med}(PLLA) > PLA_{med}(SC)$. This decrease may have occurred because brittleness increases when there is poor interfacial adhesion between components. Rigid fillers, such as SC particles, increase the stiffness of the composite but decrease the fracture toughness, which results in a more brittle material. This phenomenon explains the decreased toughness observed for $PLA_{med}(SC)$. For PLA_{low}, an increase in toughness was observed when PLLA particles were added to the matrix. A decrease in toughness compared with the neat matrix was obtained for $PLA_{low}(SC)$: $PLA_{low} < PLA_{low}(PLLA) > PLA_{low}(SC)$. The increased toughness values for $PLA_{med}(PLLA)$ and $PLA_{low}(PLLA)$ is explained by the strong interfacial adhesion between the PLLA particles and the PLA matrixes with D-lactide segments. This adhesion affects the fracture toughness. Strong adhesion leads to the increased toughness of the homocomposite. The interfacial adhesion between the particles and the matrix was confirmed by particle/matrix interfacial debonding and the subsequent appearance of voids with the straining of the crystalline matrix after tensile testing (Figure 6, blue lines). $PLA_{med}(PLLA)$ and

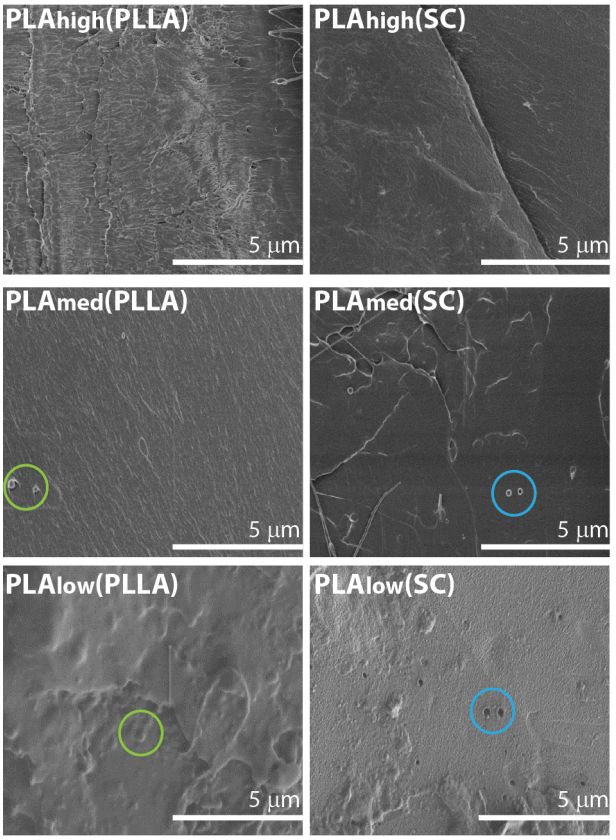

Figure 6. SEM micrographs of the cross-sectional area of the particulate-homocomposite materials after tensile testing with highlighted voids (blue line) and particles attached to the matrix (green line).

$PLA_{low}(PLLA)$ demonstrated better adhesion of the particles to their respective matrixes because of the interfacial complex crystalline structures (Figure 6, green lines). Bai et al. demonstrated improvements in PLA toughness by increasing the interfacial strength through SC crystallites.[50] In $PLA_{med}(SC)$ and $PLA_{low}(SC)$, cavities in the matrix were observed after tensile testing indicating poor adhesion between the SC particles and the matrixes. In $PLA_{high}(PLLA)$, small cavities were observed that may be attributed to nonmelted PLLA particles during the melt-blending process that was performed close to the T_m of the PLLA particles.

Heat Resistance. The thermal resistance of the homocomposite was improved with the addition of particles (Figure 7). The decomposition trace of the pure particles (Figure 7a) demonstrated that SC particles have a slightly higher thermal decomposition temperature (T_{max}) than do pure PLLA particles. The helical conformation in SC is stable at temperatures higher than the T_m because of the strong interactions between the L- and D-lactide chains. These chains reduce the molecular mobility and delay the thermal degradation. However, at temperatures much higher than the T_m of the SC, these interactions have little effect resulting in slight difference in the thermal stability between PLA

DOI: 10.1021/acssuschemeng.5b00498
ACS Sustainable Chem. Eng. 2015, 3, 2220−2231

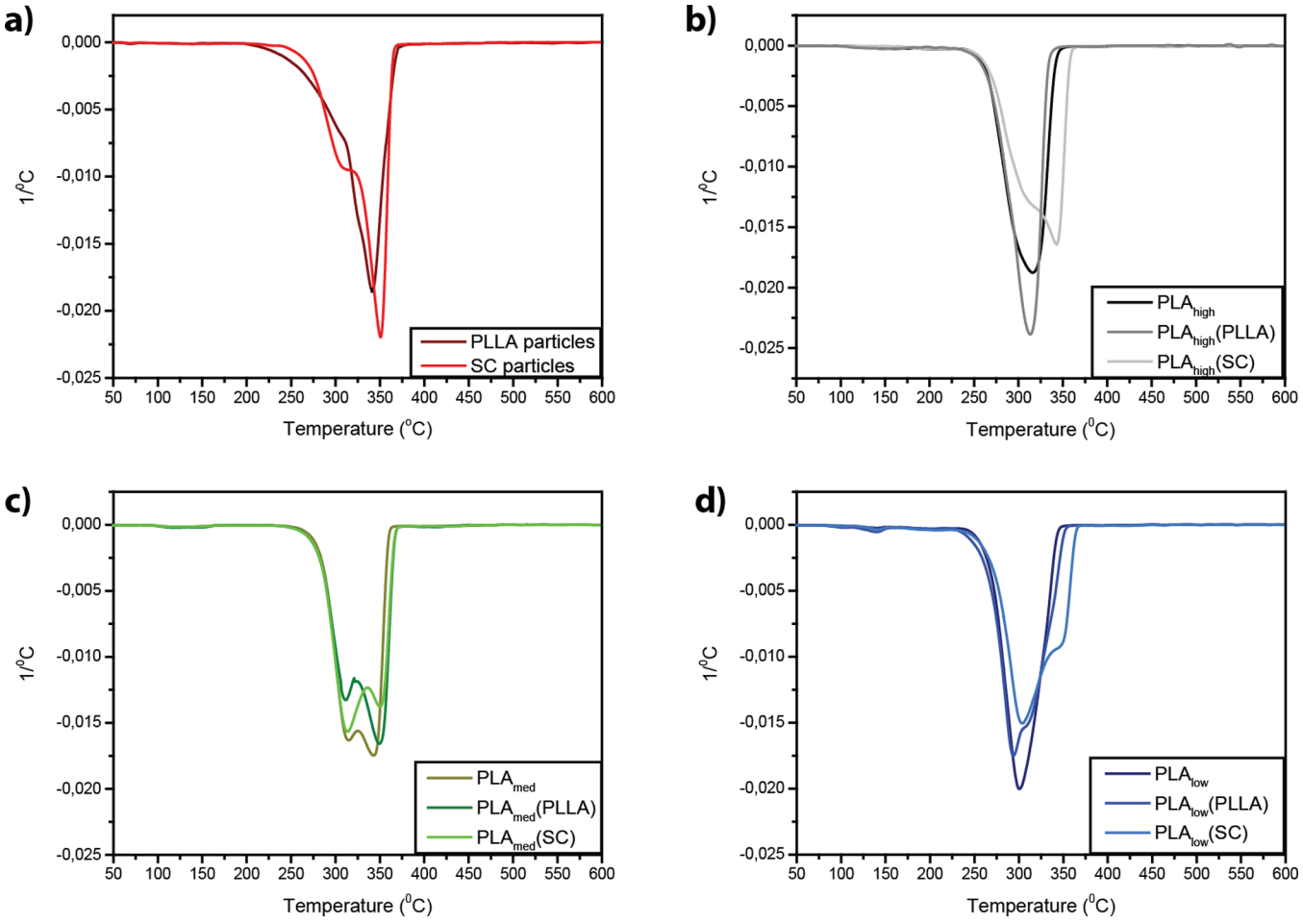

Figure 7. 1st derivatives of the decomposition traces of (a) PLLA and SC particles, (b) PLA_{high}-based particulate-homocomposites, (c) PLA_{med}-based particulate-homocomposites and (d) PLA_{low}-based particulate-homocomposites.

stereocomplex crystallites and PLA homocrystallites.[55] In PLA_{high}(SC), the first derivative of the decomposition trace demonstrated a shift toward higher temperatures with the addition of SC particles compared to PLA_{high}. No shift was observed for PLA_{high}(PLLA). PLA_{med} demonstrated double decomposition traces because of the different crystal formations. PLA_{med}(PLLA) and PLA_{med}(SC) exhibited an increase in the decomposition peak toward higher temperatures that corresponded to the decomposition of SC crystals. This peak is an indication of SC crystals formed at the interfaces between the PLLA particles and the PLA_{med} matrix. For PLA_{low}(PLLA), a small shoulder at higher temperatures appeared after the addition of PLLA particles. This shift represents SC crystal formation at the interface between the PLLA particles and the matrix. The second decomposition peak becomes more accentuated toward higher temperatures in PLA_{low}(SC) after the addition of SC particles.

Surface Topography. The surface topography of the films confirmed the particle distribution in the matrixes (Figure 8). A good distribution of both the PLLA and SC particles in the matrixes was observed. Particles were observed in PLA_{high}(PLLA). These particles are likely nonmelted PLLA particles even when the extrusion temperature for the PLA_{high} formulations was close to the T_m of the PLLA particles. The surface topography of the films depicted a specific pattern of horizontal lines in the entire area. This pattern may be attributed to the film die that was used during the extrusion.

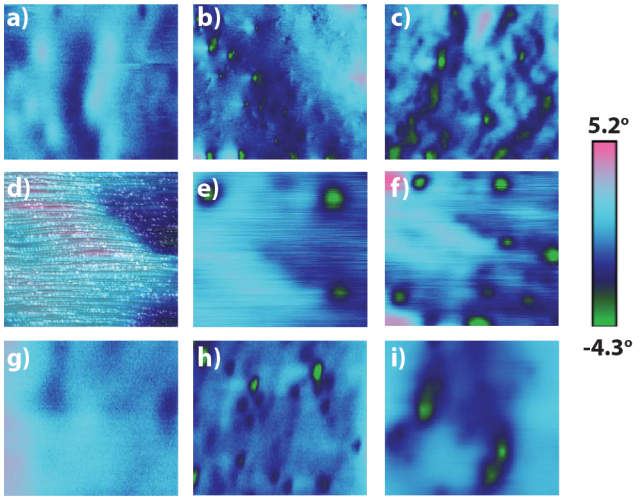

Figure 8. Representative AFM phase images of the homocomposite films after extrusion: (a) PLA_{high}, (b) PLA_{high}(PLLA), (c) PLA_{high}(SC), (d) PLA_{med}, (e) PLA_{med}(PLLA), (f) PLA_{med}(SC), (g) PLA_{low}, (h) PLA_{low}(PLLA) and (i) PLA_{low}(SC). All AFM images were scanned over an area of 2 × 2 μm.

The stereocomplexation, formed at the particle/matrix interface in PLA_{med}(PLLA) and PLA_{low}(PLLA), provided a strong matrix/filler interaction. This stereocomplexation facilitated

DOI: 10.1021/acssuschemeng.5b00498
ACS Sustainable Chem. Eng. 2015, 3, 2220−2231

the dispersion of particles in the matrix and affected the mechanical properties of the homocomposites (Figure 4).

CONCLUSIONS

Homocomposites, based solely on polylactide (PLA), that were composed of a matrix of PLA and poly-L-lactide (PLLA) or PLA stereocomplex (SC) particles were successfully prepared. Interfacial complex crystalline arrangements were obtained in various combinations of homocomposite formulations and resulted in specific thermal and mechanical properties. The stereocomplexation for some of the homocomposites formulations after processing was confirmed to occur only at the particle/matrix interface. The stereocomplexation at the particle/matrix interface was not achieved by simple physical blending of the components in the specific formulations, and nor in the pure matrixes composed of L-lactide and D-lactide units. The PLLA and SC particles functioned as nucleating agents for all matrixes and enhanced the crystallization. The E-modulus of the matrixes increased with the addition of PLLA and SC particles. Pure SC particles had a higher E-modulus than did PLLA particles. Homocomposites with rigid SC particles demonstrated a higher E-modulus than did homocomposites with PLLA particles. The tensile strength of the homocomposites was improved through the interfacial complex formation. The highest tensile strength among the homocomposite formulations was obtained when having PLLA particles into PLA matrixes due to the interfacial complex formation. The SC crystallites formed at the particle/matrix interface for the specific homocomposite formulations improved the stress transfer between the particles and the matrix. Strong interfacial adhesion was exhibited by homocomposites of PLLA particles and PLA matrixes through the interfacial stereocomplex formation. SC particles demonstrated higher decomposition trace temperatures than PLLA particles. Therefore, the heat resistance of the homocomposites was enhanced when SC particles were added to the matrixes. The strong interfacial complex adhesion in homocomposites of PLLA particles and PLA matrixes facilitated the dispersion of the particles in the matrix. The conception of homocomposites, using different structures instead of different materials, in combination with the understanding of interfacial crystalline structures formation, will enable more control over the material properties. Finally, the development of "green" homocomposites will expand the use of biobased materials in the creation of composite products, which can be chemical recycled or fully degradable, and by this contributing in the achievement of a more sustainable society.

ASSOCIATED CONTENT

Supporting Information

The Supporting Information is available free of charge on the ACS Publications website at DOI: 10.1021/acssuschemeng.5b00498.

Particle SEM micrographs, particulate-homocomposite molar masses after film extrusion, DSC thermograms of the 2nd heating scan, representative tensile strength curves and the images of the formulations with varying particle loading (PDF).

AUTHOR INFORMATION

Corresponding Author

*A.-C. Albertsson. E-mail: aila@polymer.kth.se. Tel.: +46-8-790 82 74. Fax: +46-8-20 84 77.

Notes

The authors declare no competing financial interest.

ACKNOWLEDGMENTS

The authors acknowledge the Swedish Research Council, VR (grant ID: A0347801) and the ERC Advance Grant, PARADIGM (grant agreement no.: 246776) for their financial support of this work.

REFERENCES

(1) Arias, V.; Höglund, A.; Odelius, K.; Albertsson, A.-C. Tuning the Degradation Profiles of Poly(l-lactide)-Based Materials through Miscibility. *Biomacromolecules* **2014**, *15*, 391−402.

(2) Arias, V.; Olsen, P.; Odelius, K.; Hoglund, A.; Albertsson, A.-C. Selective degradation in aliphatic block copolyesters by controlling the heterogeneity of the amorphous phase. *Polym. Chem.* **2015**, *6*, 3271−3282.

(3) Arias, V.; Odelius, K.; Albertsson, A.-C. Nano-Stereocomplexation of Polylactide (PLA) Spheres by Spray Droplet Atomization. *Macromol. Rapid Commun.* **2014**, *35*, 1949−1953.

(4) Martello, M. T.; Schneiderman, D. K.; Hillmyer, M. A. Synthesis and Melt Processing of Sustainable Poly(ε-decalactone)-block-Poly(lactide) Multiblock Thermoplastic Elastomers. *ACS Sustainable Chem. Eng.* **2014**, *2*, 2519−2526.

(5) Lebarbé, T.; Grau, E.; Gadenne, B.; Alfos, C.; Cramail, H. Synthesis of Fatty Acid-Based Polyesters and Their Blends with Poly(l-lactide) as a Way To Tailor PLLA Toughness. *ACS Sustainable Chem. Eng.* **2015**, *3*, 283−292.

(6) Olsen, P.; Borke, T.; Odelius, K.; Albertsson, A.-C. ε-Decalactone: A Thermoresilient and Toughening Comonomer to Poly(l-lactide). *Biomacromolecules* **2013**, *14*, 2883−2890.

(7) Tsuji, H.; Saeki, T.; Tsukegi, T.; Daimon, H.; Fujie, K. Comparative study on hydrolytic degradation and monomer recovery of poly(l-lactic acid) in the solid and in the melt. *Polym. Degrad. Stab.* **2008**, *93*, 1956−1963.

(8) Short, D.; Summerscales, J. Hybrids-a review: Part 1. Techniques, design and construction. *Composites* **1979**, *10*, 215−222.

(9) Dragaun, H.; Hubeny, H.; Muschik, H. Shear-induced β-form crystallization in isotactic polypropylene. *J. Polym. Sci., Polym. Phys. Ed.* **1977**, *15*, 1779−1789.

(10) Zhu, P.-w.; Tung, J.; Phillips, A.; Edward, G. Morphological Development of Oriented Isotactic Polypropylene in the Presence of a Nucleating Agent. *Macromolecules* **2006**, *39*, 1821−1831.

(11) Yan, B.; Wu, H.; Jiang, G.; Guo, S.; Huang, J. Interfacial Crystalline Structures in Injection Over-Molded Polypropylene and Bond Strength. *ACS Appl. Mater. Interfaces* **2010**, *2*, 3023−3036.

(12) Leong, Y. W.; Yamaguchi, S.; Mizoguchi, M.; Hamada, H.; Ishiaku, U. S.; Tsujii, T. The effect of molding conditions on mechanical and morphological properties at the interface of film insert injection molded polypropylene-film/polypropylene matrix. *Polym. Eng. Sci.* **2004**, *44*, 2327−2334.

(13) Yamaguchi, S.; Leong, Y. W.; Tsujii, T.; Mizoguchi, M.; Ishiaku, U. S.; Hamada, H. Effect of crystallization and interface formation mechanism on mechanical properties of film-insert injection-molded poly(propylene) (PP) film/PP substrate. *J. Appl. Polym. Sci.* **2005**, *98*, 294−301.

(14) Zhong, Y.; Fang, H.; Zhang, Y.; Wang, Z.; Yang, J.; Wang, Z. Rheologically Determined Critical Shear Rates for Shear-Induced Nucleation Rate Enhancements of Poly(lactic acid). *ACS Sustainable Chem. Eng.* **2013**, *1*, 663−672.

(15) Chung, Y.-L.; Olsson, J. V.; Li, R. J.; Frank, C. W.; Waymouth, R. M.; Billington, S. L.; Sattely, E. S. A Renewable Lignin−Lactide

DOI: 10.1021/acssuschemeng.5b00498
ACS Sustainable Chem. Eng. 2015, 3, 2220−2231

Copolymer and Application in Biobased Composites. *ACS Sustainable Chem. Eng.* **2013**, *1*, 1231−1238.
(16) Fortunati, E.; Armentano, I.; Zhou, Q.; Iannoni, A.; Saino, E.; Visai, L.; Berglund, L. A.; Kenny, J. M. Multifunctional bionanocomposite films of poly(lactic acid), cellulose nanocrystals and silver nanoparticles. *Carbohydr. Polym.* **2012**, *87*, 1596−1605.
(17) Raquez, J. M.; Murena, Y.; Goffin, A. L.; Habibi, Y.; Ruelle, B.; DeBuyl, F.; Dubois, P. Surface-modification of cellulose nanowhiskers and their use as nanoreinforcers into polylactide: A sustainably-integrated approach. *Compos. Sci. Technol.* **2012**, *72*, 544−549.
(18) Xu, H.; Xie, L.; Chen, Y.-H.; Huang, H.-D.; Xu, J.-Z.; Zhong, G.-J.; Hsiao, B. S.; Li, Z.-M. Strong Shear Flow-Driven Simultaneous Formation of Classic Shish-Kebab, Hybrid Shish-Kebab, and Transcrystallinity in Poly(lactic acid)/Natural Fiber Biocomposites. *ACS Sustainable Chem. Eng.* **2013**, *1*, 1619−1629.
(19) Magniez, K.; Voda, A. S.; Kafi, A. A.; Fichini, A.; Guo, Q.; Fox, B. L. Overcoming Interfacial Affinity Issues in Natural Fiber Reinforced Polylactide Biocomposites by Surface Adsorption of Amphiphilic Block Copolymers. *ACS Appl. Mater. Interfaces* **2013**, *5*, 276−283.
(20) Nyambo, C.; Mohanty, A. K.; Misra, M. Polylactide-Based Renewable Green Composites from Agricultural Residues and Their Hybrids. *Biomacromolecules* **2010**, *11*, 1654−1660.
(21) Gorrasi, G.; Pantani, R.; Murariu, M.; Dubois, P. PLA/Halloysite Nanocomposite Films: Water Vapor Barrier Properties and Specific Key Characteristics. *Macromol. Mater. Eng.* **2014**, *299*, 104−115.
(22) Svagan, A. J.; Åkesson, A.; Cárdenas, M.; Bulut, S.; Knudsen, J. C.; Risbo, J.; Plackett, D. Transparent Films Based on PLA and Montmorillonite with Tunable Oxygen Barrier Properties. *Biomacromolecules* **2012**, *13*, 397−405.
(23) Re, G. L.; Benali, S.; Habibi, Y.; Raquez, J.-M.; Dubois, P. Stereocomplexed PLA nanocomposites: From in situ polymerization to materials properties. *Eur. Polym. J.* **2014**, *54*, 138−150.
(24) Xu, Z.; Zhang, Y.; Wang, Z.; Sun, N.; Li, H. Enhancement of Electrical Conductivity by Changing phase Morphology for Composites Consisting of Polylactide and Poly(ε-caprolactone) Filled with Acid-Oxidized Multiwalled Carbon Nanotubes. *ACS Appl. Mater. Interfaces* **2011**, *3*, 4858−4864.
(25) Xu, Z.-H.; Niu, Y.-H.; Wang, Z.-G.; Li, H.; Yang, L.; Qiu, J.; Wang, H. Enhanced Nucleation Rate of Polylactide in Composites Assisted by Surface Acid Oxidized Carbon Nanotubes of Different Aspect Ratios. *ACS Appl. Mater. Interfaces* **2011**, *3*, 3744−3753.
(26) Krikorian, V.; Pochan, D. J. Poly (l-Lactic Acid)/Layered Silicate Nanocomposite: Fabrication, Characterization, and Properties. *Chem. Mater.* **2003**, *15*, 4317−4324.
(27) Sinha Ray, S.; Yamada, K.; Okamoto, M.; Ueda, K. New polylactide-layered silicate nanocomposites. 2. Concurrent improvements of material properties, biodegradability and melt rheology. *Polymer* **2003**, *44*, 857−866.
(28) Bussiere, P. O.; Therias, S.; Gardette, J.-L.; Murariu, M.; Dubois, P.; Baba, M. Effect of ZnO nanofillers treated with triethoxy caprylylsilane on the isothermal and non-isothermal crystallization of poly(lactic acid). *Phys. Chem. Chem. Phys.* **2012**, *14*, 12301−12308.
(29) Arias, V.; Höglund, A.; Odelius, K.; Albertsson, A.-C. Polylactides with "green" plasticizers: Influence of isomer composition. *J. Appl. Polym. Sci.* **2013**, *130*, 2962−2970.
(30) Törmälä, P. Biodegradable self-reinforced composite materials; Manufacturing structure and mechanical properties. *Clin. Mater.* **1992**, *10*, 29−34.
(31) Li, R.; Yao, D. Preparation of single poly(lactic acid) composites. *J. Appl. Polym. Sci.* **2008**, *107*, 2909−2916.
(32) Bocz, K.; Domonkos, M.; Igricz, T.; Kmetty, Á.; Bárány, T.; Marosi, G. Flame retarded self-reinforced poly(lactic acid) composites of outstanding impact resistance. *Composites, Part A* **2015**, *70*, 27−34.
(33) Okada, A.; Usuki, A. Twenty Years of Polymer-Clay Nanocomposites. *Macromol. Mater. Eng.* **2006**, *291*, 1449−1476.
(34) Odelius, K.; Plikk, P.; Albertsson, A.-C. Elastomeric Hydrolyzable Porous Scaffolds: Copolymers of Aliphatic Polyesters and a Polyether−ester. *Biomacromolecules* **2005**, *6*, 2718−2725.
(35) Feng, L.-D.; Sun, B.; Bian, X.-C.; Chen, Z.-M.; Chen, X.-S. Determination of d-lactate content in poly(lactic acid) using polarimetry. *Polym. Test.* **2010**, *29*, 771−776.
(36) Tsuji, H.; Horii, F.; Nakagawa, M.; Ikada, Y.; Odani, H.; Kitamaru, R. Stereocomplex formation between enantiomeric poly(lactic acid)s. 7. Phase structure of the stereocomplex crystallized from a dilute acetonitrile solution as studied by high-resolution solid-state carbon-13 NMR spectroscopy. *Macromolecules* **1992**, *25*, 4114−4118.
(37) Derjaguin, B. V.; Muller, V. M.; Toporov, Y. P. Effect of contact deformations on the adhesion of particles. *J. Colloid Interface Sci.* **1975**, *53*, 314−326.
(38) Muller, V. M.; Derjaguin, B. V.; Toporov, Y. P. On two methods of calculation of the force of sticking of an elastic sphere to a rigid plane. *Colloids Surf.* **1983**, *7*, 251−259.
(39) Sun, J.; Shao, J.; Huang, S.; Zhang, B.; Li, G.; Wang, X.; Chen, X. Thermostimulated crystallization of polylactide stereocomplex. *Mater. Lett.* **2012**, *89*, 169−171.
(40) Ahmed, S.; Jones, F. R. A review of particulate reinforcement theories for polymer composites. *J. Mater. Sci.* **1990**, *25*, 4933−4942.
(41) Ohtani, Y.; Okumura, K.; Kawaguchi, A. Crystallization Behavior of Amorphous Poly(l-Lactide). *J. Macromol. Sci., Part B: Phys.* **2003**, *42*, 875−888.
(42) Mauritz, K. A.; Baer, E.; Hopfinger, A. J. The epitaxial crystallization of macromolecules. *Macromol. Rev.* **1978**, *13*, 1−61.
(43) Brochu, S.; Prud'homme, R. E.; Barakat, I.; Jerome, R. Stereocomplexation and Morphology of Polylactides. *Macromolecules* **1995**, *28*, 5230−5239.
(44) Shao, J.; Sun, J.; Bian, X.; Cui, Y.; Zhou, Y.; Li, G.; Chen, X. Modified PLA Homochiral Crystallites Facilitated by the Confinement of PLA Stereocomplexes. *Macromolecules* **2013**, *46*, 6963−6971.
(45) Tsuji, H.; Tezuka, Y. Stereocomplex Formation between Enantiomeric Poly(lactic acid)s. 12. Spherulite Growth of Low-Molecular-Weight Poly(lactic acid)s from the Melt. *Biomacromolecules* **2004**, *5*, 1181−1186.
(46) Li, H.; Huneault, M. A. Effect of nucleation and plasticization on the crystallization of poly(lactic acid). *Polymer* **2007**, *48*, 6855−6866.
(47) Ikada, Y.; Jamshidi, K.; Tsuji, H.; Hyon, S. H. Stereocomplex formation between enantiomeric poly(lactides). *Macromolecules* **1987**, *20*, 904−906.
(48) Tsuji, H.; Ikada, Y.; Hyon, S.-H.; Kimura, Y.; Kitao, T. Stereocomplex formation between enantiomeric poly(lactic acid). VIII. Complex fibers spun from mixed solution of poly(D-lactic acid) and poly(L-lactic acid). *J. Appl. Polym. Sci.* **1994**, *51*, 337−344.
(49) Brizzolara, D.; Cantow, H.-J.; Diederichs, K.; Keller, E.; Domb, A. J. Mechanism of the Stereocomplex Formation between Enantiomeric Poly(lactide)s. *Macromolecules* **1996**, *29*, 191−197.
(50) Bai, H.; Bai, D.; Xiu, H.; Liu, H.; Zhang, Q.; Wang, K.; Deng, H.; Chen, F.; Fu, Q.; Chiu, F.-C. Towards high-performance poly(l-lactide)/elastomer blends with tunable interfacial adhesion and matrix crystallization via constructing stereocomplex crystallites at the interface. *RSC Adv.* **2014**, *4*, 49374−49385.
(51) Fu, S.-Y.; Feng, X.-Q.; Lauke, B.; Mai, Y.-W. Effects of particle size, particle/matrix interface adhesion and particle loading on mechanical properties of particulate−polymer composites. *Composites, Part B* **2008**, *39*, 933−961.
(52) Dekkers, M. E. J.; Heikens, D. The effect of interfacial adhesion on the tensile behavior of polystyrene−glass-bead composites. *J. Appl. Polym. Sci.* **1983**, *28*, 3809−3815.
(53) Tsuji, H.; Ikada, Y. Stereocomplex formation between enantiomeric poly(lactic acid)s. XI. Mechanical properties and morphology of solution-cast films. *Polymer* **1999**, *40*, 6699−6708.
(54) Cho, J.; Joshi, M. S.; Sun, C. T. Effect of inclusion size on mechanical properties of polymeric composites with micro and nano particles. *Compos. Sci. Technol.* **2006**, *66*, 1941−1952.

DOI: 10.1021/acssuschemeng.5b00498
ACS Sustainable Chem. Eng. 2015, 3, 2220−2231

(55) Tsuji, H.; Fukui, I. Enhanced thermal stability of poly(lactide)s in the melt by enantiomeric polymer blending. *Polymer* **2003**, *44*, 2891−2896.

DOI: 10.1021/acssuschemeng.5b00498
ACS Sustainable Chem. Eng. 2015, 3, 2220−2231